PLOS ONE

RESEARCH ARTICLE

Investigation of the active ingredients and pharmacological mechanisms of *Porana sinensis* Hemsl. Against rheumatoid arthritis using network pharmacology and experimental validation

Jing Hu[1☯], Lintao Zhao[1☯], Ning Li[1]*, Yuanyuan Yang[2], Tong Qu[1], Hui Ren[1], Xiaomin Cui[1], Hongxun Tao[3], Zhiyong Chen[1]*, Yu Peng[4]*

1 Institute of Traditional Chinese Medicine, Shaanxi Academy of Traditional Chinese Medicine, Xi'an, China, **2** Department of Traditional Chinese Medicine, Xi'an Institute for Food and Drug Control, Xi'an, China, **3** School of Food and Biological Engineering, Jiangsu University, Zhenjiang, China, **4** Jiangsu Provincial Key Laboratory of Cardiovascular and Cerebrovascular Medicine, School of Pharmacy, Nanjing Medical University, Nanjing, China

☯ These authors contributed equally to this work.
* gsshxln@163.com (NL); chenzhiyong0612@sina.com (ZC); carlylepeng@gmail.com (YP)

Citation: Hu J, Zhao L, Li N, Yang Y, Qu T, Ren H, et al. (2022) Investigation of the active ingredients and pharmacological mechanisms of *Porana sinensis* Hemsl. Against rheumatoid arthritis using network pharmacology and experimental validation. PLoS ONE 17(3): e0264786. https://doi.org/10.1371/journal.pone.0264786

Editor: Horacio Bach, University of British Columbia, CANADA

Received: August 23, 2021

Accepted: February 16, 2022

Published: March 2, 2022

Peer Review History: PLOS recognizes the benefits of transparency in the peer review process; therefore, we enable the publication of all of the content of peer review and author responses alongside final, published articles. The editorial history of this article is available here: https://doi.org/10.1371/journal.pone.0264786

Data Availability Statement: All relevant data are within the manuscript and its Supporting Information files.

Abstract

Background

Porana sinensis Hemsl. has been widely used as a substitute for Erycibes Caulis to treat rheumatoid arthritis (RA) in traditional Chinese medicine (TCM). However, little is known about the active ingredients and pharmacological mechanisms that mediate the action of *P. sinensis* against RA.

Methods

The compounds contained in *P. sinensis* were analyzed by Q Exactive Focus mass spectrometer. The active constituents and pharmacological mechanism of *P. sinensis* against RA were clarified using a network pharmacology-based investigation. LPS-induced RAW 264.7 cells was used to verify anti-inflammatory effects of the active compounds screened by network pharmacology. Collagen-induced arthritis model was used to further investigate the mechanism of *P. sinensis* against RA.

Results

The potential components and targets of *P. sinensis* against RA were analyzed using network pharmacology, and five compounds, twenty-five targets, and eight pathways were identified. Experimental validation suggested that *P. sinensis* extract and five compounds (esculetin, umbelliferone, *trans-N*-feruloyltyramine, caffeic acid and scopolin) could inhibit the release of inflammatory mediators (NO, TNF-α, IL-1β and IL-6) in LPS-induced RAW 264.7 cell. *P. sinensis* extract attenuated the severity, pathological changes, and release of

Funding: This work was financially supported by the National Natural Science Foundation of China [grant numbers 81973419, 81603264]; Key Research and Development Program of Shaanxi [grant number 2020SF-328]; Shaanxi Administration of Traditional Chinese Medicine Projects [grant number 2021-PY-003]. The funders had no role in study design, data collection and analysis, decision to publish, or preparation of the manuscript.

Competing interests: The authors have declared that no competing interests exist.

cytokines (IL-6 and HIF-1α) during RA progression by regulating the PI3K/AKT and HIF-1 pathways.

Conclusion

The study provides a basis for the application of *P. sinensis* against RA. Our findings may provide suggestions for developing *P. sinensis* into a substitute for Erycibes Caulis.

1. Introduction

With the increasing demand for traditional Chinese medicine (TCM), some natural medicinal resources are on the verge of extinction. Developing substitutes may alleviate the pressure on these endangered Chinese medicine resources [1,2]. Erycibes Caulis is widely used in treating rheumatoid arthritis (RA) in TCM [3–5]. The official species of Erycibes Caulis recorded in China Pharmacopoeia 2020 edition are *Erycibe obtusifolia* Benth. and *Erycibe schmidtii* Craib. During the course of reduction of natural sources of Erycibes Caulis, *Porana sinensis* Hemsl. has become the primary substitute on the market [3,6]. *P. sinensis*, which belongs to the family Convolvulaceae, is mainly found in limestone mountainous regions and is widely distributed in China North-Central, China South-Central, China Southeast and Vietnam [7].

Our previous studies indicated that the chemical composition of *P. sinensis* was similar to that of Erycibes Caulis, and they all contained large amounts of coumarins and quinic acid derivatives [8]. The 40% ethanolic extract of *P. sinensis* was almost non-toxic (oral administration, 5 g/kg) and exhibited anti-inflammatory and anti-nociceptive effects [3]. Xue et al. reported that 80% methanol extract of *P. sinensis* reduced the production of NO on LPS-stimulated RAW 264.7 cells, and dicaffeoylquinic acids were the active compounds [7]. Although considerable evidence exists to support *P. sinensis* used as a substitute for Erycibes Caulis, much work is still needed to demonstrate this. For example, Erycibes Caulis is widely used in treating RA in TCM; however, there has been no study of the efficacy and mechanism of *P. sinensis* for the treatment of RA.

RA is a chronic autoimmune disease, which mainly acts on synovium, cartilage and bone, resulting in the decline of physical function and quality of life [9]. At present, nonsteroidal anti-inflammatory drugs (NSAIDs) and disease-modifying anti-rheumatic drugs (DMARDs) are commonly used in the treatment of RA. Although these drugs are typically effective, they are also not satisfactory because of their low efficacy and side effects [9]. It is of great significance to develop anti-RA TCM with multi-target effect and clear pharmacological effect.

With the rapid development of bioinformatics, network pharmacology has become a hot area of pharmacology research. Because network pharmacology delivers systematic understanding of multi-component and multi-target actions, it helps clarify the effect of TCM on various diseases [10–12]. Thus, we investigated the active constituents and pharmacological mechanism of *P. sinensis* against RA by integrating network pharmacology with experimental validation.

In this work, the chemical profile of *P. sinensis* was analyzed by Q Exactive Focus mass spectrometer (MS), and 21 compounds were identified. Subsequently, these compounds were used as the basis for network pharmacological analysis. Protein-protein interaction (PPI) network for RA was established to identify potential drug targets. KEGG pathway analysis was then performed to elucidate the signaling pathway regulated by *P. sinensis*. The results of cell experiment suggested that *P. sinensis* extract and five compounds (esculetin, umbelliferone, *trans-N-*

feruloyltyramine, caffeic acid and scopolin) could inhibit the release of inflammatory mediators (NO, TNF-α, IL-1β and IL-6) in LPS-induced RAW 264.7 cell. Animal experiments showed that *P. sinensis* treated RA by modulating PI3K-Akt and HIF-1 pathways, regulating cytokine release (IL-6 and HIF-1α). The experimental results are consistent with those of network pharmacology. This study systematically explains the effective substances and mechanisms of *P. sinensis* against RA. Our findings provide feasible suggestions for developing *P. sinensis* into a substitute for Erycibes Caulis. We also expect that the research on *P. sinensis* will accelerate the rational development and utilization of plants of the genus *Porana*.

2. Materials and methods

2.1. Materials and instrumentation

Caulis of *P. sinensis* was purchased from Kunming, China, in December 2018 (lot number: 20181205). The material was identified by Dr. Zhiyong Chen and deposited at the Shaanxi Academy of Traditional Chinese Medicine. Scopolin (lot number: 16040805), scopoletin (161208), chlorogenic acid (1701904), cryptochlorogenic acid (17061401), neochlorogenic acid (17062003), 3,5-dicaffeoylquinic acid (19061201), 3,4-dicaffeoylquinic acid (17121201), 4,5-dicaffeoylquinic acid (18070401), umbelliferone (18010202), esculetin (18092803) and caffeic acid (17122804) were bought from Qiming Bioengineering Institute (Shanghai, China), *trans-N*-feruloyltyramine (W01D9Z76497) was bought from Yuanye Bioengineering Institute (Shanghai, China), and the purities of the reference compounds were all above 98%. Bovine type II collagen (20021, Chondrex, USA), Incomplete Freund's adjuvant (F5506-10ML, Sigma –Aldrich, USA). IL-1β, IL-6 and TNF-α ELISA kits were obtained from Cloud-clone Corporation (Wuhan, China). HIF-1α ELISA kits was supplied by Jiancheng Bioengineering Institute (Nanjing, China). The RAW 264.7 murine macrophage were obtained from Youersheng Bioengineering Institute (Wuhan, China). The following antibodies were used: Actin antibody (Mouse, Servicebio, Wuhan, China), PI3K antibody (Mouse, Bioss, Beijing, China), AKT antibody (Rabbit, Servicebio, Wuhan, China), p-AKT antibody (Rabbit, Affinity, USA), and HIF-1α antibody (Rabbit, Abcam, UK).

Q Exactive Focus MS (Thermo Finnigan, San Jose, USA) was applied to identify the compounds. Samples were separated on Accucure aQ C_{18} columns (2.1 mm × 150 mm, 2.6 μm) purchased from Thermo Fisher Scientific, USA. Network Pharmacology database and analysis platform: TTD (http://db.idrblab.net/ttd/); UniProt (http://www.uniprot.org/); OMIM (https://www.omim.org/); DrugBank (https://www.drugbank.ca/); GeneCards (https://www.genecards.org/); SwissTargetPrediction (http://www.swisstargetprediction.ch/); STRING (https://string-db.org/); DAVID (https://david.ncifcrf.gov/tools.jsp); R language (Version 4.0.2, https://www.r-project.org/).

2.2. Identification of compounds by LC-MS

2.2.1. Standard solutions and sample preparation. All reference compounds (1 μg/mL) were prepared in 60% methanol. Approximately 0.5 g *P. sinensis* powder (40 mesh) was extracted with 50 mL 80% methanol for 30 min by ultrasound extraction. The solution was filtered and diluted with an equal volume of 40% methanol. The sample was then filtered through 0.22-μm pore membrane.

2.2.2. Analytical conditions. Column temperature: 35˚C; flow rate: 0.3 mL/min; injection volume: 2 μL. A linear gradient elution of 0.1% formic acid aqueous (A) and methanol (B) was used. The elution program was optimized as follows: 5–25% B within 12 min, 25–38% B with over 12–20 min, 38–60% B with the range of 20–35 min. The MS parameters were optimized: spray voltage: ±3500 V; atomization temperature: 350˚C; capillary temperature: 320˚C; sheath

gas pressure: 45 arb; aux gas pressure, 15 arb; S-lens RF, 60 V; scan mode: full MS (resolution 70000) and MS/MS (17500).

2.2.3. LC-MS data analysis. The elemental compositions were calculated according to the high-precision precursor ions. All compounds reported in *P. sinensis* and *Porana* species plants were summarized to find the most reasonable molecular formula by searching literature sources. The fragmentation patterns of these compounds were used to differentiate compounds with the same formula.

2.3. Network pharmacology research of *P. sinensis* against RA

2.3.1. Targets prediction and screening. The compounds identified by UPLC-MS were used as the basis for network pharmacological analysis. This study predicted drug targets in databases such as TCMSP and GeneCards. Target prediction (TCMSP) was performed using the WES (Weighted Ensemble Similarity) model [13,14], which showed good performance with a consistency (82.83%), sensitivity (81.33%), and specificity (93.62%). We also predicted the constituent Target via the Swiss Target Prediction network server based on 2D and 3D similarity measures of known ligands [15]. The predicted targets were collated and imported into the UniProt database. Then, the mapping analysis of the normalized targets and the RA-related targets information obtained from databases (GeneCards, OMIM, TTD, and DrugBank) were conducted to screen out the potential anti-RA targets of *P. sinensis*. Finally, a component-target-disease (C-T-D) network was visualized using Cytoscape 3.6.0 plotted as an interaction network. The degree centrality (DC), betweenness centrality (BC), and closeness centrality (CC) were analyzed for each node in the C-T-D network using Cytoscape 3.6.0 software. The nodes with a DC, BC, and CC larger than the median were identified as the potential targets.

2.3.2. PPI network. The PPI network was generated by importing potential drug targets into string database. The PPI network for *P. sinensis* was then constructed using Cytoscape 3.6.0. Simultaneously, the CytoHubba plug [16] in the software was utilized to screen the hub genes, and the "Degree" algorithm was selected.

2.3.3. KEGG analysis and network construction. KEGG analysis for *P. sinensis* against RA was conducted using DAVID 6.8 database. The top 20 pathways with $P < 0.05$ were selected, and the R language was used for plotting. The component-target-pathway (C-T-P) network was generated using Cytoscape 3.6.0. A network analyzer was utilized for computing the topological parameters of the network. Generally, the highest-ranked target plays an essential role in anti-RA.

2.4. Experimental validation

2.4.1. Preparation of *P. sinensis* extract. The powder of 2 kg dry samples was extracted with 20 L 40% ethanol for 2 h by reflux extraction two times. The filtered solution was concentrated using a rotary evaporator at 50˚C. The yield of *P. sinensis* (Pse) was 13.0%. Eight active compounds in Pse were determined by HPLC according to our previous work [17], and the contents are 13.4268 mg/g (neochlorogenic acid), 12.6935 mg/g (scopolin), 48.5457 mg/g (chlorogenic acid), 8.2953 mg/g (cryptochlorogenic acid), 20.9330 mg/g (scopoletin), 28.6063 mg/g (3,4-dicaffeoylquinic acid), 13.5660 mg/g (3,5-dicaffeoylquinic acid) and 18.3498 mg/g (4,5-dicaffeoylquinic acid), respectively.

2.4.2. Effects on LPS-induced RAW 264.7 cell. *2.4.2.1. Cell culture and viability assay.* RAW 264.7 cell line was cultured in DMEM medium supplemented with 10% fetal bovine serum, and were maintained at 37˚C in a water-saturated 5% CO_2 incubator. Cells in the mid-log phase were used for further experiments. Lipopolysaccharide (LPS, 1 μg/mL) was applied

onto RAW 264.7 cell to trigger the inflammatory responses for 24 h. Methotrexate (MTX) was used as anti-inflammatory positive control.

Cell viability was measured by MTT assay (Sigma). The RAW 264.7 cells were cultured in 96-well plate at a density of 10^4 cells/well. Different concentrations of Pse and compounds were added 2 h before LPS treatment. After 24 h, 20 μL MTT (5 mg/mL) was added in each wells, and the cells continued to be incubated for 4 h. Then the formazan crystals were dissolved in DMSO and measured at 490 nm. Relative cell viability was calculated by comparing with that of the control group.

2.4.2.2. Determination of pro-inflammatory cytokines. The RAW 264.7 cells was prepared with the same procedure described above, then the cells were treated with samples (MTX, Pse, umbelliferone, caffeic acid: 120 μg/mL; scopolin, esculetin, *trans-N*-feruloyltyramine: 5 μg/mL). The supernatant was taken 24 h after administration and detected according to the instructions of NO, TNF-α, IL-1β and IL-6 kits.

2.4.3. Effects on collagen-induced arthritis model. *2.4.3.1. Animals*. The study protocol of animal experiments was reviewed and approved by the Experimental Animal Ethical Committee at the Shaanxi Academy of Traditional Chinese Medicine (license numbers AF/SL-01/01.2 and AF/SC-05/01.2). All rats received human care followed the National Institutes of Health Guide for the Care and Use of Laboratory Animals (NIH Publications No. 8023). Male SD rats (SPF grade, 180–220 g) were brought from the Experimental Animal Facilities of Xi'an Jiaotong University (SYXK2020-005). The animals were kept with a 12/12 h light/dark cycle at a temperature of 22 ± 1˚C and 65 ± 5% humidity.

2.4.3.2. Induction of collagen-induced arthritis (CIA). The 48 rats were randomly divided into six groups: the normal, model, methotrexate (1 mg/kg), high-dose (Pse, 0.6 g/kg), middle-dose (Pse, 0.3 g/kg) and low-dose (Pse, 0.15 g/kg) groups. The selection of administered doses is based on our previous studies. At these doses, the extract shows good anti-inflammatory and analgesic effects [3]. The CIA model is one of the standard RA models, which shares several pathological features with RA, such as synovial inflammatory cell infiltration, synovial hyperplasia and bone erosion [9]. The CIA model was established as previously described [18]. Type II collagen was prepared with 0.1 mol/L acetic acid at 2 mg/mL. Then, the solution was emulsified with an equal volume of incomplete Freund's adjuvant. For immunization, 0.2 mL of collagen was injected at the base of the tail of each rat. The rats were given a booster injection (0.2 mL of collagen) on day 7. On day 13, Pse (0.6, 0.3, 0.15 g/kg) was intragastric administrated once daily for 17 days, while methotrexate was given every 3 days.

During the experiment, body weights were measured every 7 days. The left hind paw's ankle circumference and the arthritis index (AI) were recorded every 4 days from day 13. The AI criteria [19]: 0, no swelling; 1, swelling or redness of digit; 2, slight swelling of the ankle; 3, gross swelling of the paw; and 4, severe arthritis of the entire paw. Hind paws were used to calculate AI. Relative organ weights were assayed as well.

2.4.3.3. Biochemical assays. On day 29, all rats were anesthetized with pentobarbital sodium, and the abdominal aorta was punctured for blood collection. The blood was centrifuged to separate the serum for ELISA testing of HIF-1α and IL-6 using assay kits.

2.4.3.4. Histopathological examination. The right hind ankle joints were harvested after serum collection, fixed in 10% formalin, and decalcified in ethylenediaminetetraacetic acid. The joints were then embedded in paraffin, stained with hematoxylin and eosin (H&E), and observed under light microscope.

2.4.3.5. Quantitative PCR analysis. The mRNA was extracted using the TRIzol reagent from the synovium of the joint. For complementary DNA (cDNA) synthesis, reverse transcriptase and 2 μg RNA were used. PCR amplification was conducted using gene-specific PCR primers provided by Wuhan Servicebio Technology (Wuhan, China). Primers used in this study are

listed in S1 Table. The amplification was performed in a 15 μL reaction volume containing 2 μL cDNA, 1.5 μL 2.5 μmol/L primers, 7.5 μL 2 × qPCR mix, and 4 μL ddH_2O. Each reaction was carried out for 40 cycles of denaturation at 95˚C for 15 s and annealing at 60˚C for 60 s. GAPDH was used as a control for normalization.

2.4.3.6. Western blot analysis. The experiment was performed following previous studies' protocol with slight modification [9]. The protein extraction of the synovium of joints was performed with RIPA lysis buffer. The lysate was then centrifuged at 4˚C, 12000 rpm for 10 min. Subsequently, the supernatant was collected and boiled for 15 min, subjected to SDS-PAGE, and transferred to PVDF membrane. After incubating with respective primary antibodies, the membrane was extensive washed with TBST, and treated with horseradish peroxidase-conjugated secondary antibodies. In the experiment, β-actin (GB12001, Wuhan Servicebio Technology) was regarded as the internal control. Protein visualization was conducted on an imaging system (Clinx, Shanghai, China).

2.5. Statistical analysis

All data were expressed as mean ± SD for each group. Comparisons between multiple groups were made with one-way ANOVA, and a value of $p < 0.05$ was considered statistically significant.

3. Results

3.1. LC-MS analysis of *P. sinensis*

The total ion chromatograms are shown in Fig 1. A total of 21 compounds and isomers from *P. sinensis* were identified, including seven coumarins (5, 8, 10, 11, 12, 13, 15), seven chlorogenic acids (2, 4, 6, 9, 16, 17, 20), one tropane alkaloid (1), two amides (19, 21), one flavonoid (18), one lignan (14) and two other compounds (3, 7). Twelve compounds were unambiguously identified as neochlorogenic acid (2), chlorogenic acid (4), scopolin (5), cryptochlorogenic acid (6), caffeic acid (7), umbelliferone (8), scopoletin (10), esculetin (15), 3,4-dicaffeoylquinic acid (16), 3,5-dicaffeoylquinic acid (17), 4,5-dicaffeoylquinic acid (20),

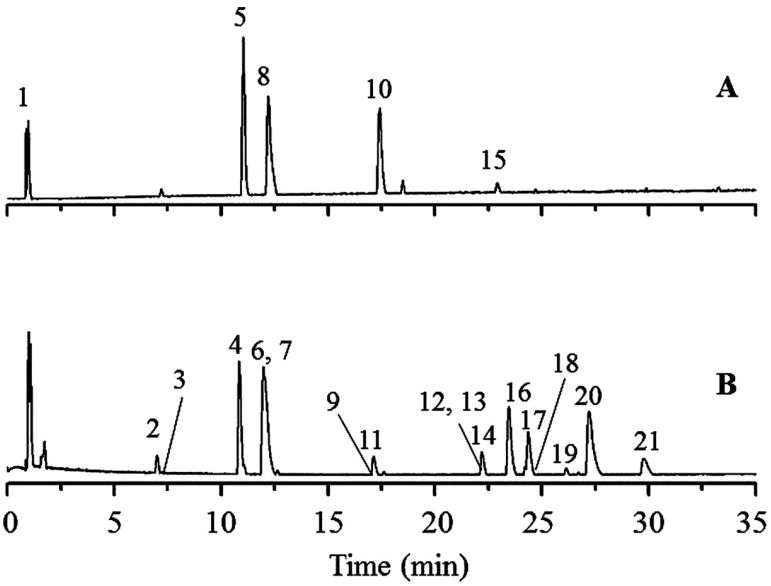

Fig 1. Total ion chromatograms of *P. sinensis* in positive ion (A) and negative ion (B) modes.

https://doi.org/10.1371/journal.pone.0264786.g001

Table 1. Identification of chemical constituents from *P. sinensis* by UPLC-MS.

No.	t_R (min)	Observed *m/z*	Calculated *m/z*	Mode	Error (ppm)	Molecular formula	Fragment ions (*m/z*)	Identification	References
1	0.97	144.1015	144.1019	$[M+H]^+$	-2.77	$C_7H_{13}NO_2$	144.1015, 126.0910, 108.0806, 98.0962, 84.0806, 68.0696	baogongteng C or erycibelline	[17]
2*	7.00	353.0862	353.0868	$[M-H]^-$	-1.70	$C_{16}H_{18}O_9$	353.0859, 191.0546, 179.0334, 173.0443, 161.0227, 135.0435	neochlorogenic acid	[7,8]
3	7.28	153.0177	153.0182	$[M-H]^-$	-3.27	$C_7H_6O_4$	153.0178, 141.9110, 123.0074, 109.0278, 61.9858	3,4-dihydroxybenzoic acid	[7,8]
4*	10.86	353.0862	353.0868	$[M-H]^-$	-1.70	$C_{16}H_{18}O_9$	191.0560, 179.0347, 161.0242	chlorogenic acid	[7,8]
5*	11.04	355.1014	355.1024	$[M+H]^+$	-2.82	$C_{16}H_{18}O_9$	193.0493, 178.0259, 165.0543, 133.0282	scopolin	[7,8]
6*	11.98	353.0862	353.0868	$[M-H]^-$	-1.70	$C_{16}H_{18}O_9$	191.0545, 179.0347, 173.0452, 135.0434	cryptochlorogenic acid	[7,8]
7*	12.07	179.0334	179.0339	$[M-H]^-$	-2.79	$C_9H_8O_4$	179.0334, 135.0435	caffeic acid	[7]
8*	12.21	163.0383	163.0388	$[M+H]^+$	-3.07	$C_9H_6O_3$	163.0385, 145.0281, 135.0437, 117.0332, 107.0490, 89.0384	umbelliferone	[20]
9	17.13	367.1017	367.1024	$[M-H]^-$	-1.91	$C_{17}H_{20}O_9$	191.0545, 173.0438, 135.0356, 111.0435, 93.0329, 87.0071	methyl chlorogenate	[21]
10*	17.44	193.0492	193.0495	$[M+H]^+$	-1.55	$C_{10}H_8O_4$	193.0491, 178.0255, 165.0539, 149.0591, 137.0595, 133.0281	scopoletin	[3]
11	19.85	695.1804	695.1818	$[M-H]^-$	-2.01	$C_{31}H_{36}O_{18}$	359.0966, 335.0766, 197.0441, 173.0437, 153.0538, 135.0438	eryciboside F	[21]
12	21.60	665.1702	665.1712	$[M-H]^-$	-1.50	$C_{30}H_{34}O_{17}$	198.0475, 191.0334, 176.0099, 153.0540, 121.0278	eryciboside A or B or C	[21]
13	21.75	635.1597	635.1607	$[M-H]^-$	-1.57	$C_{29}H_{32}O_{16}$	191.0334, 167.0334, 121.0433	eryciboside D or E	[21]
14	22.19	595.2012	595.2021	$[M-H]^-$	-1.51	$C_{28}H_{36}O_{14}$	447.4385, 433.1486, 418.1223, 403.1426, 373.1277, 358.1036, 239.7386, 181.0488, 139.0023	aketrilignoside B	[21]
15*	22.92	179.0333	179.0338	$[M+H]^+$	-2.79	$C_9H_6O_4$	179.0333, 151.0386, 133.0280, 123.0436	esculetin	[22]
16*	23.46	515.1171	515.1184	$[M-H]^-$	-2.52	$C_{25}H_{24}O_{12}$	353.0859, 335.0760, 191.0546, 179.0334, 173.0439, 161.0228, 135.0435, 93.0329	3,4-dicaffeoylquinic acid	[7,8]
17*	24.38	515.1171	515.1184	$[M-H]^-$	-2.52	$C_{25}H_{24}O_{12}$	353.0862, 191.0545, 179.0333, 173.0437, 135.0434	3,5-dicaffeoylquinic acid	[7,8]
18	24.67	287.0548	287.0550	$[M-H]^-$	-0.697	$C_{15}H_{12}O_6$	243.0648, 199.0746, 177.0539, 163.0380, 137.0223, 119.0485, 93.0330, 61.9869	eriodictyol	[21]
19	25.87	282.1123	282.1125	$[M-H]^-$	-0.709	$C_{17}H_{17}O_3N$	282.1122, 197.9011, 162.0543, 1485.0278, 136.0750, 119.0485	*trans-N*-(p-coumaroyl) tyramine	[20]
20*	27.23	515.1171	515.1184	$[M-H]^-$	-2.52	$C_{25}H_{24}O_{12}$	353.0858, 191.0545, 179.0333, 173.0438, 135.0434, 93.0327	4,5-dicaffeoylquinic acid	[7,8]
21*	29.85	312.1246	312.1238	$[M-H]^-$	2.56	$C_{18}H_{19}O_4N$	312.1238, 297.1001, 190.0508, 178.0506, 148.0528, 135.0451	*trans-N*-feruloyltyramine	[20]

* Compared with reference compounds.

https://doi.org/10.1371/journal.pone.0264786.t001

and *trans-N*-feruloyltyramine (21) by comparisons with reference compounds. Data for all compounds are listed in Table 1.

3.2. Network pharmacology analysis of *P. sinensis*

3.2.1. C-T-D network construction and core target screening. Through Swiss Target Prediction and DrugBank reverse Prediction, 466 potential targets for 21 chemical components were obtained. The 466 potential targets were mapped to RA targets, and 293 common potential targets against RA were obtained. Using these targets as network nodes, Cytoscape

Table 2. The topological parameter analysis of 10 compounds in *P. sinensis* against rheumatoid arthritis.

No.	compounds	molecular formula	Betweenness centrality (BC)	Closeness centrality (CC)	Degree centrality (DC)
1	Scopolin	$C_{16}H_{18}O_9$	0.00554748	0.3665	45
2	Scopoletin	$C_{10}H_8O_4$	0.01196908	0.3842	86
3	Neochlorogenicacid	$C_{16}H_{18}O_9$	0.00316416	0.3642	40
4	4,5-Dicaffeoylquinicacid	$C_{25}H_{24}O_{12}$	0.00264869	0.3639	44
5	3,5-Dicaffeoylquinicacid	$C_{25}H_{24}O_{12}$	0.00366490	0.3639	42
6	3,4-Dicaffeoylquinicacid	$C_{25}H_{24}O_{12}$	0.00264869	0.3639	44
7	Esculetin	$C_9H_6O_3$	0.02573882	0.4049	116
8	Caffeic acid	$C_9H_8O_4$	0.01098960	0.3787	64
9	Umbelliferone	$C_9H_6O_3$	0.01219321	0.3861	81
10	*trans-N*-feruloyltyramine	$C_{18}H_{19}O_4N$	0.02687441	0.4122	102

https://doi.org/10.1371/journal.pone.0264786.t002

3.6.0 software was used to analyze network topology parameters. The results showed that the median DC was 41, the average BC was 0.0026, and the average CC was 0.3639 for the compounds; the median DC was 2, the average BC was 0.0013, and the average CC was 0.4897 for the 293 common targets. There were ten compounds and 112 common targets with DC, BC, and CC values higher than the median, shown in S1 Fig, **Tables** 2 and 3.

3.2.2. Construction of the PPI network. Searching for proteins playing important roles in the PPI network, we uploaded the 112 anti-RA targets to the STRING database to observe these protein interaction relationships. Then, we imported the obtained TSV file into Cytoscape 3.6.0 to build the PPI network. Using the Cytohubba plugin, the greater the node's degree value, the redder its color, the more important it is in the network (S2 Fig). The hub genes include CAPDH (Degree = 92), AKT1 (Degree = 91), GASP3 (Degree = 81), EGFR (Degree = 78), SRC (Degree = 76), HSP90AA1 (Degree = 75), MAPK1 (Degree = 72), TNF (Degree = 67), ESR1 (Degree = 67), STAT3 (Degree = 66).

Table 3. The topological parameter analysis of 112 targets with rheumatoid arthritis for *P. sinensis*.

NO.	UniProt	Gene names	Betweenness centrality (BC)	Closeness centrality (CC)	Degree centrality (DC)
1	Q14790	CASP8	0.00441081	0.49481865	6
2	P08246	ELANE	0.00673174	0.49739583	8
3	P08183	ABCB1	0.00741662	0.49739583	8
4	P42574	CASP3	0.00719441	0.49739583	8
5	P17252	PRKCA	0.00719441	0.49739583	8
6	Q05655	PRKCD	0.00541423	0.4961039	7
7	P08253	MMP2	0.01899941	0.5	10
8	P05067	APP	0.00673172	0.49739583	8
9	P15121	AKR1B1	0.02883723	0.50395778	13
10	P21964	COMT	0.00114453	0.49226804	4
11	P56817	BACE1	0.01344752	0.49869452	9
12	P04626	ERBB2	0.00064866	0.49100257	3
13	P09874	PARP1	0.00114453	0.49226804	4
14	P03372	ESR1	0.00200793	0.49354005	5
15	P27338	MAOB	0.00224914	0.49354005	5
16	P05177	CYP1A2	0.00144712	0.49226804	4
17	P22303	ACHE	0.00078702	0.49100257	3

(*Continued*)

Table 3. (Continued)

NO.	UniProt	Gene names	Betweenness centrality (BC)	Closeness centrality (CC)	Degree centrality (DC)
18	P35968	KDR	0.00570423	0.4961039	7
19	P12931	SRC	0.00247146	0.49354005	5
20	P00390	GSR	0.00114453	0.49226804	4
21	P49841	GSK3B	0.00114453	0.49226804	4
22	P09769	FGR	0.00114453	0.49226804	4
23	P0DMV8	HSPA1A	0.00114453	0.49226804	4
24	P53350	PLK1	0.00114453	0.49226804	4
25	Q05397	PTK2	0.00064866	0.49100257	3
26	P09917	ALOX5	0.00154686	0.49226804	4
27	Q92731	ESR2	0.00200793	0.49354005	5
28	P42262	GRIA2	0.00032983	0.48974359	2
29	P07550	ADRB2	0.00091322	0.49100257	3
30	P00533	EGFR	0.00455135	0.4961039	7
31	P28482	MAPK1	0.00130213	0.49100257	3
32	Q07820	MCL1	0.00067511	0.48974359	2
33	P04406	GAPDH	0.00067511	0.48974359	2
34	P01375	TNF	0.00116211	0.49100257	3
35	P11142	HSPA8	0.00067511	0.48974359	2
36	P20248	CCNA2	0.00234162	0.49354005	5
37	P78396	CCNA1	0.00234162	0.49354005	5
38	P24941	CDK2	0.00334262	0.49481865	6
39	P14635	CCNB1	0.00116211	0.49100257	3
40	P06493	CDK1	0.00116211	0.49100257	3
41	P11802	CDK4	0.00334262	0.49481865	6
42	P24385	CCND1	0.00234162	0.49354005	5
43	P11021	HSPA5	0.00067511	0.48974359	2
44	P60568	IL2	0.00067511	0.48974359	2
45	P19367	HK1	0.00067511	0.48974359	2
46	P52789	HK2	0.00067511	0.48974359	2
47	P30542	ADORA1	0.01223823	0.49481865	6
48	P0DMS8	ADORA3	0.0151816	0.49739583	8
49	P10275	AR	0.00067511	0.48974359	2
50	P35869	AHR	0.00111812	0.49100257	3
51	P35354	PTGS2	0.00546993	0.4961039	7
52	P18031	PTPN1	0.00140827	0.4961039	7
53	Q02750	MAP2K1	0.00184084	0.49100257	3
54	P29323	EPHB2	0.00028174	0.48974359	2
55	P04818	TYMS	0.00028174	0.48974359	2
56	O14672	ADAM10	0.00028174	0.48974359	2
57	P55072	VCP	0.00028174	0.48974359	2
58	P08238	HSP90AB1	0.00028174	0.48974359	2
59	P14625	HSP90B1	0.00028174	0.48974359	2
60	P50281	MMP14	0.00028174	0.48974359	2
61	P15144	ANPEP	0.00028174	0.48974359	2
62	AGTR1	AGTR1	0.00028174	0.48974359	2
63	P11387	TOP1	0.00023523	0.49100257	3
64	Q13547	HDAC1	0.00028174	0.48974359	2

(*Continued*)

Table 3. (Continued)

NO.	UniProt	Gene names	Betweenness centrality (BC)	Closeness centrality (CC)	Degree centrality (DC)
65	P35462	DRD3	0.00028174	0.48974359	2
66	P14416	DRD2	0.00028174	0.48974359	2
67	O60760	HPGDS	0.00028174	0.48974359	2
68	P23443	RPS6KB1	0.00028174	0.48974359	2
69	Q05193	DNM1	0.00028174	0.48974359	2
70	P42345	MTOR	0.00028174	0.48974359	2
71	O14757	CHEK1	0.00028174	0.48974359	2
72	Q92769	HDAC2	0.00034993	0.48974359	2
73	P19838	NFKB1	0.00034993	0.48974359	2
74	P40763	STAT3	0.00045826	0.48974359	2
75	Q16236	NFE2L2	0.00045826	0.48974359	2
76	O15054	KDM6B	0.00045826	0.48974359	2
77	P42336	PIK3CA	0.00045826	0.48974359	2
78	P08684	CYP3A4	0.00045826	0.48974359	2
79	P42338	PIK3CB	0.00045826	0.48974359	2
80	P06239	LCK	0.00045826	0.48974359	2
81	O00206	TLR4	0.00045826	0.48974359	2
82	P14780	MMP9	0.00329356	0.49226804	4
83	P37840	SNCA	0.00066095	0.49100257	3
84	Q14289	PTK2B	0.00066095	0.49100257	3
85	P09619	PDGFRB	0.00066095	0.49100257	3
86	P08069	IGF1R	0.00023292	0.48974359	2
87	P07948	LYN	0.00066095	0.49100257	3
88	P31749	AKT1	0.00066095	0.49100257	3
89	P11388	TOP2A	0.00023292	0.48974359	2
90	P05771	PRKCB	0.00023292	0.48974359	2
91	P17612	PRKACA	0.00023292	0.48974359	2
92	O75469	NR1I2	0.00023292	0.48974359	2
93	P15559	NQO1	0.00023292	0.48974359	2
94	P23458	JAK1	0.00023292	0.48974359	2
95	P07900	HSP90AA1	0.00128134	0.49226804	4
96	Q99527	GPER1	0.00023292	0.48974359	2
97	P26358	DNMT1	0.00023292	0.48974359	2
98	Q16678	CYP1B1	0.00023292	0.48974359	2
99	Q00534	CDK6	0.00023292	0.48974359	2
101	P60709	ACTB	0.00023292	0.48974359	2
102	P08254	MMP3	0.00068484	0.49100257	3
103	P06400	RB1	0.00023292	0.48974359	2
104	P38936	CDKN1A	0.00023292	0.48974359	2
105	P10415	BCL2	0.00023292	0.48974359	2
106	P08473	MME	0.00074482	0.48974359	2
107	P29317	EPHA2	0.00127883	0.49100257	3
108	P00519	ABL1	0.00127883	0.49100257	3
109	P05556	ITGB1	0.00074482	0.48974359	2
110	P16109	SELP	0.00141277	0.49100257	3
111	P16581	SELE	0.00141277	0.49100257	3
112	P02766	TTR	0.00141277	0.49100257	3

https://doi.org/10.1371/journal.pone.0264786.t003

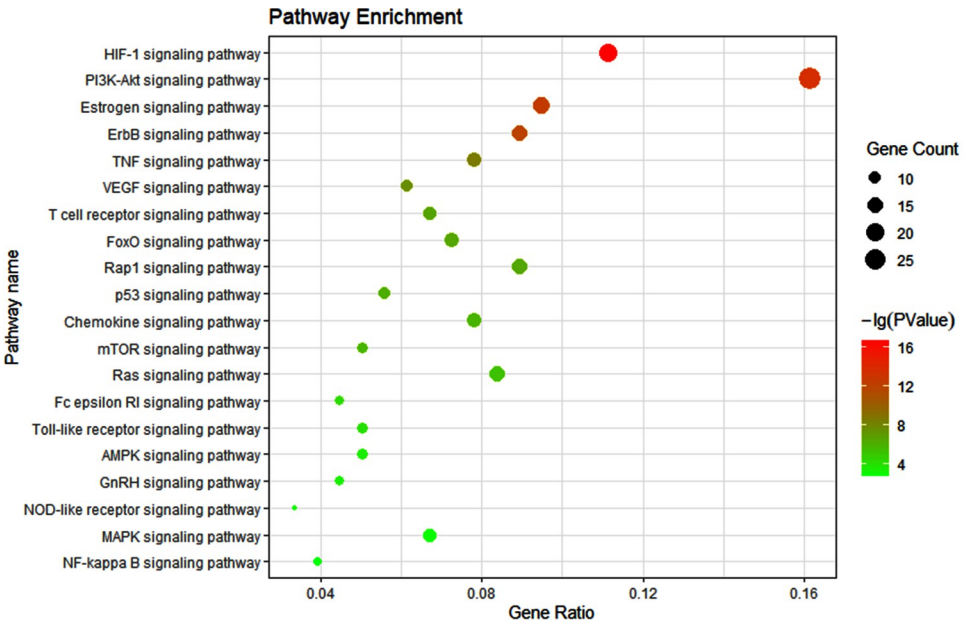

Fig 2. KEGG pathway enrichment analysis of 112 target genes.

https://doi.org/10.1371/journal.pone.0264786.g002

3.2.3. KEGG analysis and C-T-P construction. The 112 targets were mapped to 122 pathways using DAVID. Unrelated pathways, such as "Pathways in cancer", "Hepatitis B" and "Bladder cancer" were excluded. The top 20 KEGG pathways were obtained based on *P*-value (**S3 Fig**, **S2 Table**), shown in **Fig 2**. A total of 64 targets were directly connected to the top 20 pathways. Most of these pathways are involved in inflammation, such as PI3K-Akt, HIF-1, ErbB, Rap1, TNF, VEGF, Ras signaling pathways.

The C-T-P network for the *P. sinensis*-mediated treatment of RA is shown in **Fig 3**. The network comprises 94 nodes (10 compounds, 64 targets, and 20 pathways) and 400 edges. The green triangle represents the compounds, the yellow diamond denotes the potential targets, and the purple V graphics represents the pathways. The topological parameters of C-T-P were

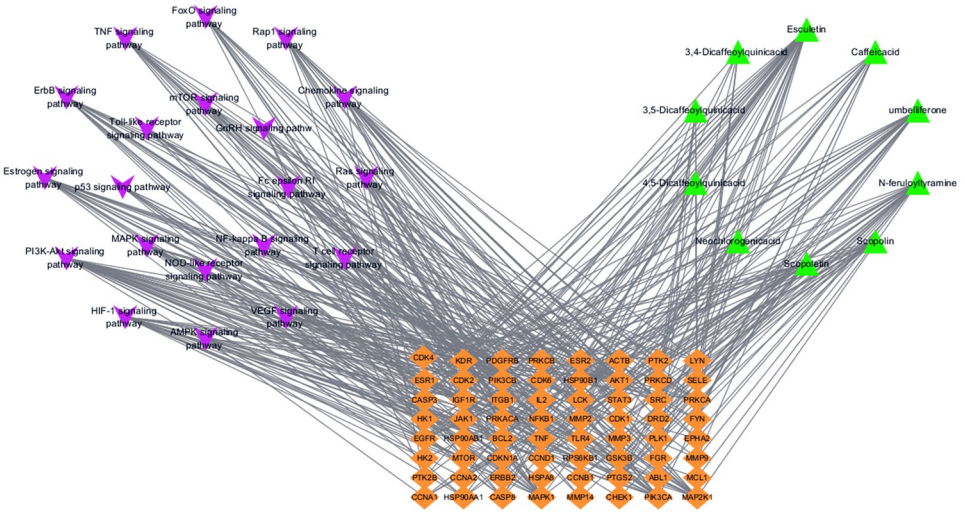

Fig 3. The C-T-P network for *P. sinensis* in treatment of rheumatoid arthritis.

https://doi.org/10.1371/journal.pone.0264786.g003

calculated using the Network Analyzer (Table 4). The results show that the median DC was 16, the median BC was 0.0351, and the median CC was 0.4115 for the compounds. There were 5 compounds with DC, BC and CC values higher than the median: esculetin (DC = 30, BC = 0.1328, CC = 0.4898), umbelliferone (DC = 20, BC = 0.0481, CC = 0.4348), *trans-N*-feruloyltyramine (DC = 21, BC = 0.0917, CC = 0.4471), caffeic acid (DC = 16, BC = 0.0351, CC = 0.4115) and scopolin (DC = 16, BC = 0.0547, CC = 0.4152). The median values of DC, BC, and CC were 7, 0.0093 and 0.4155 for targets nodes, respectively. There were 25 targets that exhibited high topological values. For the pathway nodes, the median values of DC, BC

Table 4. The topological parameter analysis of C-T-P for *P. sinensis* in treatment of rheumatoid arthritis.

Number	Node	Betweenness centrality (BC)	Closeness centrality (CC)	Degree centrality (DC)
1	*trans-N*-feruloyltyramine	0.0917	0.4471	21
2	umbelliferone	0.0481	0.4348	20
3	Caffeic acid	0.0351	0.4115	13
4	Esculetin	0.1328	0.4898	30
5	Scopolin	0.0547	0.4152	16
6	Ras signaling pathway	0.0225	0.4189	15
7	Chemokine signaling pathway	0.0244	0.4043	14
8	Rap1 signaling pathway	0.0380	0.4189	16
9	TNF signaling pathway	0.0460	0.4189	14
10	ErbB signaling pathway	0.0275	0.4227	16
11	Estrogen signaling pathway	0.0531	0.4227	17
12	PI3K-Akt signaling pathway	0.1271	0.4745	29
13	HIF-1 signaling pathway	0.0593	0.4387	19
14	MAP2K1	0.0379	0.4947	16
15	RPS6KB1	0.0057	0.3974	6
16	MTOR	0.0057	0.3974	6
17	NFKB1	0.0211	0.4471	11
18	PIK3CA	0.0331	0.4947	16
19	PIK3CB	0.0331	0.4947	16
20	PDGFRB	0.0044	0.4009	6
21	IGF1R	0.0064	0.4079	7
22	AKT1	0.0462	0.5054	18
23	PRKCB	0.0060	0.4009	8
24	PRKACA	0.0043	0.3875	6
25	HSP90AA1	0.0095	0.4306	6
26	CDKN1A	0.0071	0.4079	6
27	CASP3	0.0195	0.4115	8
28	PRKCA	0.0353	0.4346	12
29	KDR	0.0156	0.4152	9
30	SRC	0.0153	0.4189	10
31	GSK3B	0.0068	0.4079	7
32	EGFR	0.0445	0.4895	15
33	MAPK1	0.0558	0.5167	19
34	TNF	0.0185	0.4043	10
35	CDK2	0.0152	0.4471	8
36	CDK4	0.0172	0.4515	8
37	CCND1	0.0127	0.4266	8
38	PTGS2	0.0229	0.4387	9

https://doi.org/10.1371/journal.pone.0264786.t004

and CC were 12, 0.0224 and 0.4043. There were 8 pathways that exhibited high topological values.

3.3. Experimental validation for *P. sinensis* against RA

3.3.1. Effects on LPS-induced RAW 264.7 cell. Prior to validation of the effects of Pse and five active compounds on LPS-induced RAW 264.7 cell, we first analyzed their cellular toxicities using the MTT cell viability assay. The results showed that RAW 264.7 cell viability was 83.6% after induction with LPS (1 μg/mL) alone, so we chose this concentration for subsequent experiments. Based on the anti-inflammatory activity and cytotoxicity, we selected the dose concentration of the samples (S4 Fig). As shown in Fig 4, Pse and the five compounds screened by network pharmacology all showed good anti-inflammatory activities, and the inhibition effect of Pse on NO and IL-6 was better than umbelliferone and caffeic acid at the same concentration. Inhibitory effects of *trans-N*-feruloyltyramine on IL-1β and IL-6 were not obvious.

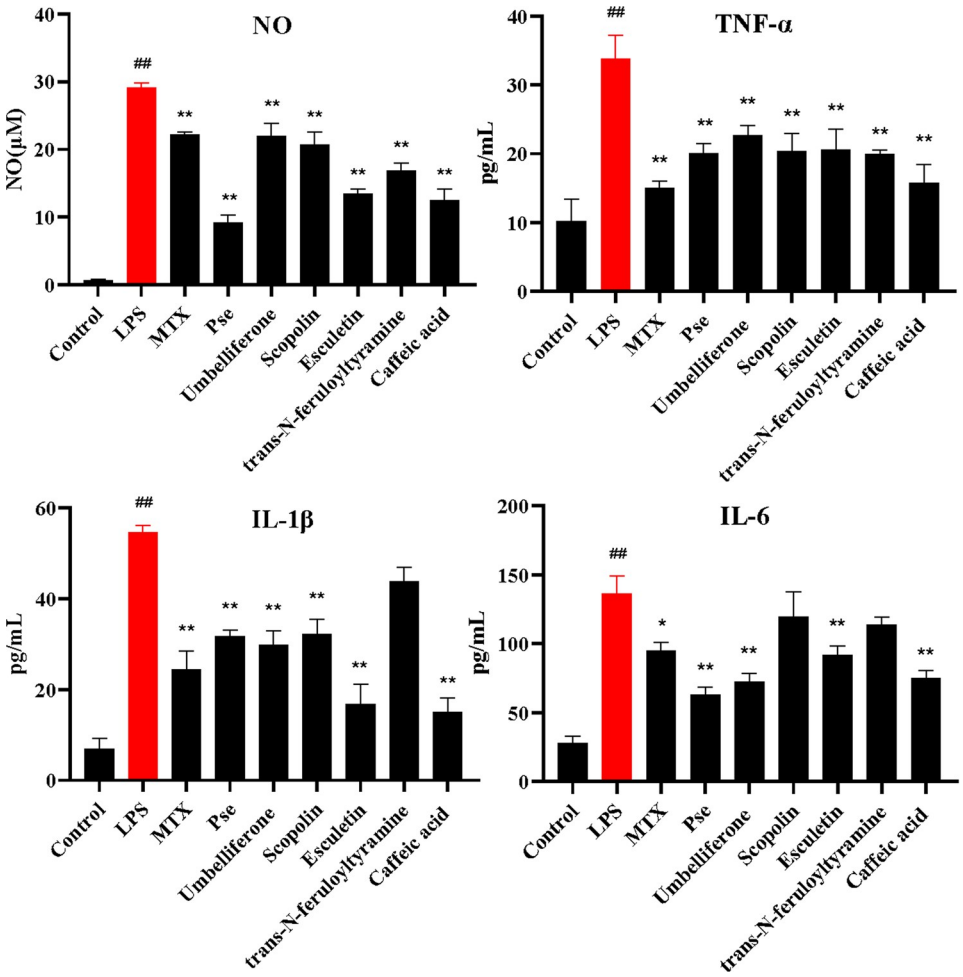

Fig 4. Inhibitory effect of *P. sinensis* extract (Pse), methotrexate (MTX) and five compounds (esculetin, umbelliferone, *trans-N*-feruloyltyramine, caffeic acid and scopolin) on the release of inflammatory mediators (NO, TNF-α, IL-1β and IL-6) in LPS-induced RAW 264.7 cell. $^{*}P < 0.05$ and $^{**}P < 0.01$ compared with model group; $^{\#}P < 0.05$ and $^{\#\#}P < 0.01$ compared with normal group.

https://doi.org/10.1371/journal.pone.0264786.g004

3.3.2. Effects on collagen-induced arthritis model. *3.3.2.1. Effects of P. sinensis on ankle circumference and AI.* Red swelling in the paws of model rats was first observed on day 11 following CIA-induced modeling. As shown in S5 Fig, edema of the left hind paw and AI of rats were significantly different between normal and model groups on day 13, which represents the successful model. The arthritis severity in the model group reached a peak on Day 21. Pse (0.6 g/kg) can suppress the paw swelling and AI on day 29.

3.3.2.2. Effects of P. sinensis on body weight and relative organ weight. As shown in S5 Fig, body weight in normal group rats increased more than CIA rats ($p < 0.01$), while Pse treated rats (0.6 g/kg, 0.3 g/kg) did not achieve a significant difference from model group rats ($p > 0.05$). The weight gain of rats in the methotrexate treated group was less than that in the model group ($p < 0.05$). As shown in Table 5, the spleen's relative organ weight in methotrexate treated rats was significantly higher than rats of other groups ($p < 0.01$).

3.3.2.3. Effect of P. sinensis on serum cytokine levels. As shown in S6 Fig, collagen-induced the significant production of HIF-1α and IL-6 compared with the normal group. Pse (0.6 g/kg) inhibited the collagen-induced production of HIF-1α and IL-6.

3.3.2.4. Effect of P. sinensis on histopathological changes. The histopathological changes of ankle joints in each group are shown in Fig 5. In the model group, inflammatory infiltration, synovial hyperplasia, and cartilage degradation were observed in the ankle joint. Methotrexate and Pse significantly attenuated the synovial hyperplasia and cartilage degradation.

3.3.2.5. Effects of P. sinensis on the mRNA expression. As shown in S7 Fig, compared with the normal group, the mRNA levels of HIF-1α, PI3K, and AKT in the model group were significantly increased ($P < 0.05$). The high-dose group of Pse has an effect of decreasing the mRNA levels of HIF-1α, PI3K, and AKT ($P < 0.05$).

3.3.2.6. Effects of P. sinensis on the protein expression levels. As shown in Fig 6, the expression levels of PI3K, AKT, p-AKT, and HIF-1α proteins were significantly increased in the synovium of CIA model rats, compared to the normal group ($p < 0.01$). After the administration of Pse (0.6 g/kg), their expression levels were significantly reduced ($p < 0.05$).

4. Discussion

The similarity of chemical compositions is an essential indicator for judging the rationality of substitutes. In this study, a total of 21 compounds from *P. sinensis* were identified by UPLC-MS, including seven coumarins, seven chlorogenic acids, one tropane alkaloid, two amides, one flavonoid, one lignan, and two other compounds. By comparing with other studies [4,8,23,24], we discovered the chemical composition of *P. sinensis* is similar to that of *E. obtusifolia* and *E. schmidtii*. It should be noted that there are few reports on the systematic

Table 5. Relative organ weights in rats. Data represent the mean ± SD.

Relative organ weight (g/100 g)	Normal	Model	Methotrexate (1 mg/kg)	Pse (0.6 g/kg)	Pse (0.3 g/kg)	Pse (0.15 g/kg)
Kidney	0.63±0.03	0.71±0.04##	0.71±0.06	0.75±0.03	0.72±0.05	0.69±0.06
Heart	0.32±0.04	0.33±0.03	0.35±0.06	0.34±0.03	0.33±0.03	0.34±0.05
Liver	3.50±0.25	3.07±0.15##	2.83±0.45	3.01±0.18	3.42±0.42*	3.17±0.43
Spleen	0.18±0.04	0.20±0.02	0.35±0.15**	0.20±0.03	0.20±0.03	0.19±0.02
Lung	0.53±0.07	0.67±0.12##	0.76±0.07	0.63±0.10	0.60±0.08	0.57±0.10

*$P < 0.05$ and

**$P < 0.01$ compared with model group

#$P < 0.05$ and

##$P < 0.01$ compared with normal group.

https://doi.org/10.1371/journal.pone.0264786.t005

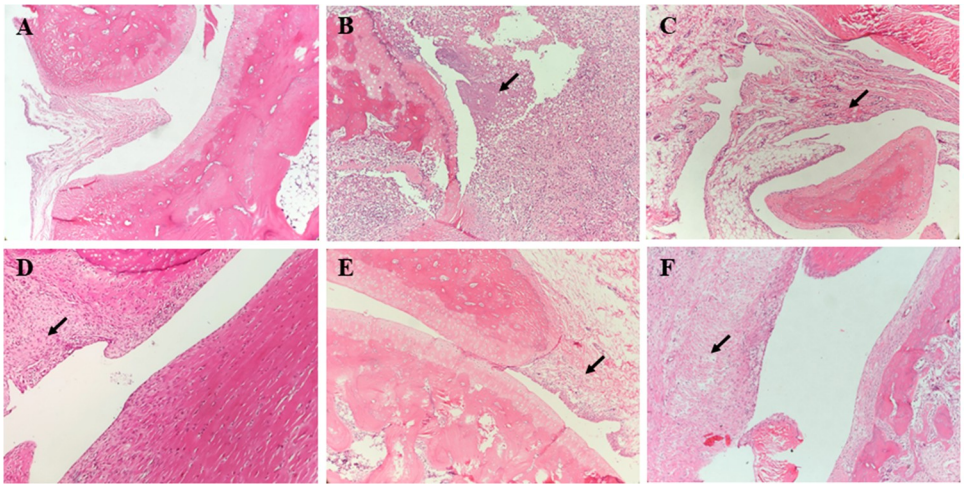

Fig 5. Histopathological examination of ankle joints (×100). (A) normal group, (B) model group, (C) methotrexate group, (D) *P. sinensis* extract group (0.6 g/kg), (E) *P. sinensis* extract group (0.3 g/kg), (F) *P. sinensis* extract group (0.15 g/kg).

https://doi.org/10.1371/journal.pone.0264786.g005

isolation of *P. sinensis*; only nine compounds were reported from this plant [20]. Therefore, systematic studies on the phytochemistry of *P. sinensis* need to be carried out. Future phytochemical studies of *P. sinensis* should focus on separating and identifying distinct chemical components to clarify the chemical similarities and differences between *P. sinensis* and Erycibes Caulis.

The potential components and targets of *P. sinensis* against RA were analyzed using a network pharmacology approach, and five compounds, twenty-five targets, and eight pathways were finally obtained. Esculetin was shown to possess an anti-inflammatory effect by suppressing the HIF-1α signaling pathways [25]. Caffeic acid attenuated hepatocellular carcinoma cells' angiogenesis by reducing JNK-1-mediated HIF-1α stabilization [26]. Umbelliferone was useful for treating arthritis by suppressing the MAPK/NF-κB pathway [27]. In this study, KEGG analysis and C-T-P network showed that *P. sinensis* regulated the PI3K/Akt, HIF-1, Estrogen, Rap1 signaling pathways and so on. Recent studies demonstrated that PI3K/AKT pathway inhibits apoptosis in chondrocytes, and modulation of the pathway has been proposed as a

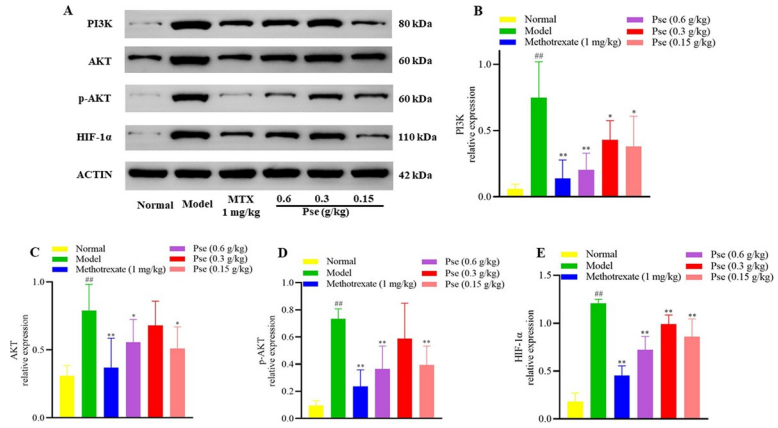

Fig 6. Effects of *P. sinensis* extract (Pse) on the expression levels of PI3K, AKT, p-AKT, and HIF-1α proteins. The specific bands of proteins (A), the expression levels of proteins (B~E).

https://doi.org/10.1371/journal.pone.0264786.g006

potential therapy against RA [28,29]. HIF-1α can increase the production of inflammatory cytokines, and promote angiogenesis in RA patients [30,31]. The maintenance of Rap1 signaling in T cells can reduce the incidence rate and severity of CIA [32].

Macrophages play an important role in the pathogenesis of RA, and are the main source of inflammatory cytokines (such as NO, TNF-α, IL-1β, and IL-6) [33]. Therefore, we chose LPS-induced RAW 264.7 cells to verify the results of network pharmacology in vitro. A large number of literatures have reported the levels of TNF-α, IL-1β and IL-6 were significantly increased in serum of patients with RA [34]. At the same time, TNF is an important target of *P. sinensis* for the treatment of RA in our network pharmacology research. Therefore, these indexes were selected to verify the anti-inflammatory activity of Pse and five active compounds. It was reported that caffeic acid and caffeoylquinic acids could be active compounds of the anti-inflammatory potential of *P. sinensis* [7]. In this study, coumarins (esculetin, umbelliferone and scopolin) and amides (*trans-N*-feruloyltyramine) from *P. sinensis* showed good anti-inflammatory activities, especially amides, which should be attached great attentions to quality control of *P. sinensis* in the future.

Adjuvant-induced arthritis (AIA) and CIA models are classic animal models for RA research. However, AIA is different from RA in that it lacks a chronic pathological process [35]. At present, the CIA is recognized as the best RA model. We verified the computational prediction mechanisms of *P. sinensis* against RA based on the CIA rat model. The PI3K/AKT pathway is closely related to RA by deregulating activated immune cells' proliferation and synovial fibroblasts [28]. Zou et al [36] reported that HIF-1 levels in the peripheral serum of CIA rats positively correlated with AI, and the CIA rat model regulated the expression of HIF-1α proteins via PI3K pathway. Combined with network pharmacology and literature reports, the PI3K/AKT and HIF-1 pathway was selected for confirmation. The results suggested that Pse attenuates the severity, pathological changes, and the release of cytokines (IL-6 and HIF-1α) during RA progression in a dose-dependent manner. Western blot analysis demonstrated that Pse significantly reduced protein levels of PI3K, p-AKT, and HIF-1α in the inflamed joints of CIA rats. The experimental results are consistent with those of network pharmacology. As a positive control, methotrexate significantly inhibited the arthritic response of rats; however, the relative organ weight of the spleen was significantly higher than in rats of other groups, and the weight gain of rats was less than that of the model group, which may be side effects of methotrexate. By contrast, *P. sinensis* treated RA without these side effects. This suggests *P. sinensis* may be a better choice than methotrexate when treating RA.

In recent years, with the decrease of natural resources of Erycibes Caulis, *P. sinensis* has been used as the primary substitute. The study on the anti-rheumatic effect of *P. sinensis* provided evidence for its use as a substitute. The genus *Porana* is widely distributed globally; however, there are few medicinal uses. We expect this study on *P. sinensis* will accelerate the rational development and utilization of genus *Porana* plants.

5. Conclusion

We identified 21 compounds containing in *P. sinensis* by UPLC-MS and offered evidence that *P. sinensis* reverses the pathological events during RA progression by regulating the PI3K/AKT and HIF-1 signaling pathways. *P. sinensis* extract and five compounds (esculetin, umbelliferone, *trans-N*-feruloyltyramine, caffeic acid and scopolin) could inhibit the release of inflammatory mediators (NO, TNF-α, IL-1β and IL-6) in LPS-induced RAW 264.7 cell. These findings provide the experimental basis for the application of *P. sinensis* against RA. In addition, we expect that our findings may help develop *P. sinensis* into a substitute for Erycibes Caulis, thereby setting an example for the study of substitutes for TCM.

Supporting information

S1 Fig. The C-T-D network for *P. sinensis* in treatment of rheumatoid arthritis.
(PDF)

S2 Fig. The protein-protein interaction (PPI) network.
(PDF)

S3 Fig. The KEGG pathway for *P. sinensis* against rheumatoid arthritis.
(PDF)

S4 Fig. Effects of cytotoxicity on RAW264.7 cells of *P. sinensis* extract (Pse) and its effective constituents ($^{**}P < 0.01$).
(PDF)

S5 Fig. Effects of *P. sinensis* extract (Pse) on ankle circumference (A), arthritis index (B) and body weight (C) of rats. Values shown are mean ± SD (n = 8); $^{*}P < 0.05$ and $^{**}P < 0.01$ compared with model group; $^{\#}P < 0.05$ and $^{\#\#}P < 0.01$ compared with normal group.
(PDF)

S6 Fig. Effects of *P. sinensis* extract (Pse) on HIF-1α and IL-6 levels in collagen-induced arthritis rats.
(PDF)

S7 Fig. Effects of *P. sinensis* extract (Pse) on mRNA levels of HIF-1α (A), PI3K (B) and AKT (C).
(PDF)

S1 Table. Summary of gene-specific real-time PCR primer sequences.
(DOC)

S2 Table. The information of top 20 significant KEGG enrichment analysis.
(DOC)

S1 File.
(ZIP)

Acknowledgments

We are thankful to Dr. Xia Du from Shaanxi Academy of Traditional Chinese Medicine for providing technical assistance with network pharmacology.

Author Contributions

Data curation: Jing Hu, Yuanyuan Yang, Tong Qu.

Investigation: Jing Hu, Lintao Zhao, Ning Li.

Project administration: Zhiyong Chen.

Validation: Hui Ren, Xiaomin Cui.

Writing – original draft: Zhiyong Chen.

Writing – review & editing: Hongxun Tao, Yu Peng.

References

1. Li M, Au KY, Lam H, Cheng L, Jiang RW, But PP, et al. Identification of Baiying (Herba Solani Lyrati) commodity and its toxic substitute Xungufeng (Herba Aristolochiae Mollissimae) using DNA barcoding and chemical profiling techniques. Food Chem. 2012; 135: 1653–1658. https://doi.org/10.1016/j.foodchem.2012.06.049 PMID: 22953906.
2. Padma V, Ashwini G, Vidyashankar R, Kuruvilla G. Evaluation of traditional anthelmintic herbs as substitutes for the endangered Embelia ribes, using Caenorhabditis elegans model. Curr Sci. 2013; 105: 1593–1598.
3. Chen Z, Liao L, Zhang Z, Wu L, Wang Z. Comparison of active constituents, acute toxicity, anti-nociceptive and anti-inflammatory activities of *Porana sinensis* Hemsl., *Erycibe obtusifolia* Benth. and *Erycibe schmidtii* Craib. J Ethnopharmacol. 2013; 150: 501–506. https://doi.org/10.1016/j.jep.2013.08.059 PMID: 24055469.
4. Ren W, Wang Y, He Q, Zhou Y, Li C, Wang W, et al. Chemical composition of *Erycibe schmidtii* and antiproliferative activity of scopoletin on immature dendritic cells. Nat Prod Res. 2020; 34: 2581–2588. https://doi.org/10.1080/14786419.2018.1547292 PMID: 30661400.
5. Xue Q, Fan H, Li K, Yang L, Sun L, Liu Y. Comparative evaluations on phenolic antioxidants of nine adulterants and anti-inflammation of four alternatives with their original herb *Erycibe schmidtii*. RSC Adv. 2017; 7: 51151–51161. https://doi.org/10.1039/c7ra10767f.
6. Wu LH, Zhu EY, Zhang ZJ, Wang ZT. Investigating original plant of Caulis Erycibes in Guangxi and identifying mainstream variety of Caulis Erycibes in market. Chinese Traditional and Herbal Drugs. 2005; 36: 1398–1400. https://doi.org/10.3321/j.issn:0253-2670.2005.09.044.
7. Xue Q, Yin P, Li K, Fan H, Yang L, Cao X, et al. Identification of bioactive phenolics from *Porana sinensis* Hemsl. stem by UPLC-QTOF-MS/MS and the confirmation of anti-inflammatory indicators using LPS-induced RAW264.7 cells. Inflammopharmacology. 2019; 27: 1055–1069. https://doi.org/10.1007/s10787-018-00558-1 PMID: 30689101.
8. Chen Z, Liao L, Yang Y, Zhang Z, Wang Z. Different fingerprinting strategies to differentiate *Porana sinensis* and plants of Erycibe by high-performance liquid chromatography with diode array detection, ultra high performance liquid chromatography with tandem quadrupole mass spectrometry, and chemometrics. J Sep Sci. 2015; 38: 231–238. https://doi.org/10.1002/jssc.201400861 PMID: 25376844.
9. Xiong H, Ding X, Wang H, Jiang H, Wu X, Tu C, et al. Tibetan medicine Kuan-Jin-Teng exerts anti-arthritic effects on collagen-induced arthritis rats via inhibition the production of pro-inflammatory cytokines and down-regulation of MAPK signaling pathway. Phytomedicine. 2019; 57: 271–281. https://doi.org/10.1016/j.phymed.2018.12.023 PMID: 30802713.
10. Du X, Zhao L, Yang Y, Zhang Z, Hu J, Ren H, et al. Investigation of the mechanism of action of *Porana sinensis* Hemsl. against gout arthritis using network pharmacology and experimental validation. J Ethnopharmacol. 2020; 252: 112606. https://doi.org/10.1016/j.jep.2020.112606 PMID: 31988013.
11. Li W, Mao XA, Wu HC, Guo MA, Su XA, Lu JB, et al. Deciphering the chemical profile and pharmacological mechanisms of Baihu-Guizhi decoction using ultra-fast liquid chromatography-quadrupole-time-of-flight tandem mass spectrometry coupled with network pharmacology-based investigation. Phytomedicine. 2020; 67: 153156. https://doi.org/10.1016/j.phymed.2019.153156 PMID: 31901568.
12. Mou X, Zhou DY, Zhou D, Liu K, Chen LJ, Liu WH. A bioinformatics and network pharmacology approach to the mechanisms of action of Shenxiao decoction for the treatment of diabetic nephropathy. Phytomedicine. 2020; 69: 153192. https://doi.org/10.1016/j.phymed.2020.153192 PMID: 32200292.
13. Ru J, Li P, Wang J, Zhou W, Li B, Huang C, et al. TCMSP: a database of systems pharmacology for drug discovery from herbal medicines. J Cheminform. 2014; 6: 13. https://doi.org/10.1186/1758-2946-6-13 PMID: 24735618.
14. Yu H, Chen J, Xu X, Li Y, Zhao H, Fang Y, et al. A Systematic Prediction of Multiple Drug-Target Interactions from Chemical, Genomic, and Pharmacological Data. PloS one. 2012; 7: e37608. https://doi.org/10.1371/journal.pone.0037608 PMID: 22666371.
15. Gfeller D, Grosdidier A, Wirth M, Daina A, Michielin O, Zoete V. SwissTargetPrediction: a web server for target prediction of bioactive small molecules. Nucl Acids Res. 2014; 42: 32–38. https://doi.org/10.1093/nar/gku293 PMID: 24792161.
16. Chen DQ, Kong XS, Shen XB, Huang MZ, Zheng JP, Sun J, et al. Identification of Differentially Expressed Genes and Signaling Pathways in Acute Myocardial Infarction Based on Integrated Bioinformatics Analysis. Cardiovasc Ther. 2019; 2019: 8490707. https://doi.org/10.1155/2019/8490707 PMID: 31772617.
17. Chen Z, Wang M, Yang Y, Du X, Zhang Z, Li Y. Qualitative and quantitative analysis of *Porana sinensis* Hemsl by UHPLC-Q-Exactive MS, TLC autographic method and DART-MS. Phytochem Analysis. 2018; 30: 311–319. https://doi.org/10.1002/pca.2814 PMID: 30569488.

18. Wang Q, Ye C, Sun S, Li R, Shi X, Wang S, et al. Curcumin attenuates collagen-induced rat arthritis via anti-inflammatory and apoptotic effects. Int Immunopharmacol. 2019; 72: 292–300. https://doi.org/10.1016/j.intimp.2019.04.027 PMID: 31005039.
19. Liu B, Liu F, Wang R, Xue J, Liu W, Feng F, et al. Chemical constituents of total alkaloids from picrasma quassioides and its effects on collagen induced arthritis in rats. Journal of China Pharmaceutical University. 2019; 50: 585–592. https://doi.org/10.11665/j.issn.1000-5048.20190512.
20. Zhang CF, Zhang ZJ, Zhang M, Wang ZT. Studies on Chemical Constituents in Stems of *Porana sinensis* Hemsl. Chinese Pharmaceutical Journal. 2006; 41: 94–96. https://doi.org/10.3321/j.issn:1001-2494.2006.02.004.
21. Peng Y, Tao H, Yang Y, Gao Y, Ren H, Hu J, et al. Chemical compositions, pharmacological activities, quality control studies of Erycibes plants, and the development of their substitutes. Phytother Res. 2021; 35: 4049–4074. https://doi.org/10.1002/ptr.7070 PMID: 33724590.
22. Chen Z, Yang Y, Tao H, Liao L, Li Y, Zhang Z. Direct Analysis in Real-time Mass Spectrometry for Rapid Identification of Traditional Chinese Medicines with Coumarins as Primary Characteristics. Phytochem Anal. 2017; 28: 137–143. https://doi.org/10.1002/pca.2650 PMID: 27880856.
23. Chen Z, Tao H, Liao L, Zhang Z, Wang Z. Quick identification of xanthine oxidase inhibitor and antioxidant from Erycibe obtusifolia by a drug discovery platform composed of multiple mass spectrometric platforms and thin-layer chromatography bioautography. J Sep Sci. 2014; 37: 2253–2259. https://doi.org/10.1002/jssc.201400342 PMID: 24895238.
24. Choi JY, Lee JW, Jang H, Kim JG, Lee MK, Hong JT, et al. Quinic acid esters from *Erycibe obtusifolia* with antioxidant and tyrosinase inhibitory activities. Nat Prod Res. 2019; 1–7. https://doi.org/10.1080/14786419.2019.1684285 PMID: 31680567.
25. Yum S, Jeong S, Lee S, Kim W, Nam J, Jung Y. HIF-prolyl hydroxylase is a potential molecular target for esculetin-mediated anti-colitic effect. Fitoterapia. 2015; 103: 55–62. https://doi.org/10.1016/j.fitote.2015.03.013 PMID: 25797536.
26. Gu W, Yang Y, Zhang C, Zhang Y, Chen L, Shen J, et al. Caffeic acid attenuates the angiogenic function of hepatocellular carcinoma cells via reduction in JNK-1-mediated HIF-1α stabilization in hypoxia. Rsc Adv. 2016; 6: 82774–82782. https://doi.org/10.1039/C6RA07703J.
27. Liu O, Dan Y, Shao Z, Yang S, Yang C, Liu G, et al. Effect of umbelliferone on adjuvant-induced arthritis in rats by MAPK/NF-κB pathway. Drug Des Devel Ther. 2019; 13: 1163–1170. https://doi.org/10.2147/DDDT.S190155 PMID: 31043769.
28. Malemud CJ. The PI3K/Akt/PTEN/mTOR pathway: a fruitful target for inducing cell death in rheumatoid arthritis? Future Med Chem. 2015; 7: 1137–1147. https://doi.org/10.4155/fmc.15.55 PMID: 26132523.
29. Qu Y, Wu J, Deng JX, Zhang YP, Liang WY, Jiang ZL, et al. MicroRNA-126 affects rheumatoid arthritis synovial fibroblast proliferation and apoptosis by targeting PIK3R2 and regulating PI3K-AKT signal pathway. Oncotarget. 2016; 7: 74217–74226. https://doi.org/10.18632/oncotarget.12487 PMID: 27729613.
30. Park SY, Lee SW, Kim HY, Lee WS, Hong KW, Kim CD. HMGB1 induces angiogenesis in rheumatoid arthritis via HIF-1 activation. Eur J Immunol. 2015; 45: 1216–1227. https://doi.org/10.1002/eji.201444908 PMID: 25545169.
31. Xing R, Jin Y, Sun L, Yang L, Li C, Li Z, et al. Interleukin-21 induces migration and invasion of fibroblast-like synoviocytes from patients with rheumatoid arthritis. Clin Exp Immunol. 2016; 184: 147–158. https://doi.org/10.1111/cei.12751 PMID: 26646950.
32. Abreu J, Krausz S, Dontje W, Grabiec AM, Dquist KA. Sustained T cell Rap1 signaling is protective in the collagen-induced arthritis model of rheumatoid arthritis. Arthritis Rheumatol. 2014; 62: 3289–3299. https://doi.org/10.1002/art.27656 PMID: 20662068.
33. Han J, Wan M, Ma Z, Hu C, Yi H. Prediction of Targets of Curculigoside A in Osteoporosis and Rheumatoid Arthritis Using Network Pharmacology and Experimental Verification. Drug Des Devel Ther. 2020; 14: 5235–5250. https://doi.org/10.2147/DDDT.S282112 PMID: 33273808.
34. Zheng Y, Sun L, Jiang T, Zhang D, Nie H. Tnfα promotes th17 cell differentiation through il-6 and il-1β produced by monocytes in rheumatoid arthritis. J Immunol Res. 2014; 11: 385352. https://doi.org/10.1155/2014/385352 PMID: 25436214.
35. Du CC, Tan YQ, Shen JY, Huang M, Ge FJ, Hong K, et al. Effect and Mechanism of Dihydroartemisinin on Rheumatoid Arthritis Animal Models. Chinese Journal of Experimental Traditional Medical Formulae. 2019; 25: 48–56. https://doi.org/10.13422/j.cnki.syfjx.20191002.
36. Zou L, Zhang G, Liu L, Chen C, Cai J. Relationship between PI3K pathway and angiogenesis in CIA rat synovium. Am J Transl Res. 2016; 8: 3141–3147 PMID: 27508035.